Recycling of nitrogen and light noble gases in the Central American subduction zone: constraints from 15 N 15 N

Jabrane Labidi, E.D. Young, T.P. Fischer, P.H. Barry, C.J. Ballentine, J.M. de Moor

Recycling of nitrogen and light noble gases in the Central American subduction zone: constraints from $^{15}N^{15}N$

J. Labidi[1], E.D. Young[2], T.P. Fischer[3], P.H. Barry[4], C.J. Ballentine[5], J.M. de Moor[3,6]

[1] Université de Paris, Institut de physique du globe de Paris, CNRS, Paris, France

[2] Department of Earth, Planetary, and Space Sciences, UCLA, Los Angeles, CA, USA.

[3] Department of Earth and Planetary Sciences, University of New Mexico, Albuquerque, NM 87131-1116, USA

[4] Marine Chemistry and Geochemistry Department, Woods Hole Oceanographic Institution, Woods Hole MA 02543 USA

[5] Department of Earth Sciences, University of Oxford, OX1 3AN, UK

[6]Observatorio Volcanológico y Sismológico de Costa Rica (OVSICORI), Universidad Nacional, Costa Rica

Abstract

How much nitrogen and light noble gases are recycled in modern subduction zones is unclear. Fumaroles act as a means for passive degassing in arcs. They receive variable contributions of volatiles from arc magmas, themselves sourced from the mantle wedge. The gas compositions reflect the extent of volatile enrichment in sub-arc mantle sources and constrain slab dehydration. However, contributions from atmospheric components in fumaroles are unavoidable. For N_2, neon and argon, the atmospheric components are challenging to discern from slab-derived components. Here, we report $^{15}N^{15}N$ measurements from eight fumaroles and seven bubbling springs, along the Central American arc. Our new $^{15}N^{15}N$ data are coupled with noble gases measurements and show that air-derived components in volcanic gas discharges can easily be underestimated, in both fumaroles and springs, using conventional stable isotope or noble gases methods. We

show that, in the absence of $^{15}N^{15}N$ data, previously used tracers for air (e.g., $\delta^{15}N$, N_2/Ar, N_2/He, among others) may lead to erroneous conclusions regarding the origin of volatiles in mixed gases. In contrast, $^{15}N^{15}N$ data provide quantitative constraints on the nature and contributions of both atmospheric and magmatic components. Most springs are heavily dominated by air-derived N_2, while fumaroles show substantial contributions of volcanic endmembers. Based on the fumarole data, we show that magma sources beneath the central American arc are enriched in all volatiles relative to ^{3}He, by two to three orders of magnitude compared to the MORB source. We use new $^{15}N^{15}N$ data to obtain source $N_2/^3$He, ^{3}He/^{36}Ar and ^{3}He/^{22}Ne ratios which we then use to compute volcanic N_2, Ar and Ne degassing fluxes. Using this approach, we show that outgassing fluxes appear to match subduction fluxes in the Central America subduction zone. We determine an N_2 outgassing flux of between 4.0 x 10^8 and 1.0 x10^9 mol N_2/y, comparable to the subduction flux of 5.7 x 10^8 mol N_2/yr determined previously. We obtain a similar conclusion for ^{22}Ne and ^{36}Ar. Overall, the volatile fluxes in the central American subduction zone no longer seem to require net transfer of N_2, Ar, and Ne, to the deep mantle.

1. Introduction

The origin of volatiles emitted from convergent margins provides fundamental constraints on how plate tectonics redistributes volatiles between terrestrial reservoirs (Bekaert et al., 2020; Hilton et al., 2002; Plank et al., 2013). The nitrogen cycle is under-constrained, partly because quantifying degassing N_2 fluxes in arcs is challenging. For instance, basalt glasses are virtually absent in subduction zones, impeding quantification of nitrogen elemental abundances in the underlying mantle wedge. The systematic study of

metamorphic rocks has suggested nitrogen is quantitatively retained within minerals in downgoing slabs (Bebout et al., 2013; Busigny et al., 2003). The latter is based on the composition of rocks from the European alps, where sediments underwent metamorphism in a cold subduction zone (630 °C at 100 km, Busigny et al., 2003). In those rocks, nitrogen is hosted in the structures of clay minerals including micas and illites, as NH_4^+ substituting for potassium (Bebout et al., 1992, Busigny et al., 2003; Nieder et al., 2011). Experimental work confirms that the fluid/rock nitrogen partition coefficient in a cold P-T pathway is in favor of N retention in minerals (Jackson et al., 2021). However, under warmer conditions, fluid/rock partitioning favors N accumulation in fluids, potentially limiting nitrogen subduction to the mantle (Jackson et al., 2021). Subduction temperature gradients were likely steeper in most of the Proterozoic and Archean (Martin and Moyen, 2002). Therefore, it is unclear how modern fluxes determined in cold subduction zones should be extrapolated back into deep time.

The Central American Volcanic Arc (CAVA) is relatively well-characterized with evidence for sedimentary and igneous components from the slab variably contributing to mantle sources across the arc (Patino et al., 2000). It is a "warm" subduction zone, with predicted slab interface temperatures of ~ 800 °C at 100 km depth beneath Costa Rica (Peacock et al., 2005), resulting in sporadic slab melting (Hoernle et al., 2008). Thus, it may be considered an analog for subduction zones at a time when subduction temperature gradients were steeper. In Central America, metamorphic rocks cannot be used to constrain net subduction fluxes because no section of metasediments having undergone the subduction P-T pathway is known to occur in the geological record. Instead, net subduction fluxes of volatiles are estimated from comparing their concentrations and isotopic

compositions in the offshore altered oceanic crust (Li and Bebout, 2005, Busigny et al., 2019) with their concentrations and isotopic compositions in arc fumaroles that represent volcanic outgassing fluxes. This mass balance calculation can be hampered by ubiquitous infiltration of air into most fumaroles, as evidenced by noble gases systematics: although fumaroles typically show mantle-like helium isotope ratios, neon and argon budgets are overwhelmed by atmospheric components (Hilton et al., 2002; Snyder et al., 2003). This is also a problem for nitrogen. Historically, SO_2/N_2 ratios from fumaroles and the overall SO_2 outgassing flux has been used to determine a total N_2 volcanic outgassing flux for the central American arc, yielding a value of 1.7×10^9 mol N_2/yr, or 3.4×10^9 mol N/yr (Hilton et al., 2002, Fischer et al., 2002). This is comparable to an estimate of the central American subduction nitrogen flux of ~1.1×10^9 mol N/yr (equivalent to ~5.7×10^8 mol N_2/yr) from Busigny et al. (2019). These flux estimates are given with no uncertainties, but they appear comparable within a factor of 2. Taken at face value, this would support inefficient N recycling from the surface to the deep mantle. However, fumaroles incorporate air-derived N_2, after the infiltration of meteoric water within subsurface hydrothermal systems and/or because of sampling techniques (Fischer et al., 2002). Thus, the outgassing N_2 fluxes based on raw N_2/SO_2 ratios in fumaroles are overestimates of the outgassing N_2 flux. As a remedy, the volcanic fraction of N_2 in fumaroles was quantified on the basis of N_2/Ar ratios: air-saturated waters have a known N_2/Ar ratio of ~40 at STP but most hydrothermal gases in the CAVA have ratios > 80 (Hilton et al., 2002; Fischer et al., 2002, Elkins et al., 2006, Snyder et al., 2003; Zimmer et al., 2004). The N_2 amount in excess of air-saturated water, termed N_2*, was suggested to reflect the volcanic N_2 fraction (Hilton et al., 2002, Fischer et al., 2002). A volcanic nitrogen degassing flux of 2.9×10^8 mol N_2/year was estimated for the

central American arc (Fischer et al., 2002). This degassing flux estimate is lower by a factor of 2 than the subduction nitrogen flux of ~5.7 x 10^8 mol N_2/year (or ~1.1 x 10^9 mol N/yr), suggesting N_2 sequestration into the deep mantle by subduction, even in a warm subduction zone (Busigny et al., 2019; Li and Bebout, 2005).

Here, we take a new approach to constrain the origin of N_2 as well as light noble gases in CAVA fumaroles and springs. We use the newly-developed $^{15}N^{15}N$ tracer of atmospheric contamination (Labidi et al., 2020; Yeung et al., 2017; Young et al., 2016). Specifically, we use Δ_{30}, the $^{15}N^{15}N$ concentration relative to a random distribution of ^{14}N and ^{15}N atoms among N_2 molecules, as a tracer of surficial atmospheric contamination. The Δ_{30} tracer is defined as $\Delta_{30} = {}^{30}R/({}^{15}R)^2 - 1$ (‰), where $^{30}R = {}^{15}N^{15}N/{}^{14}N^{14}N$ and $^{15}R = {}^{15}N/{}^{14}N$ for the gas of interest. At relevant temperatures ranging from 200 to 1000 °C, equilibrium among N_2 isotopologues results in Δ_{30} values from 0.5 to 0.1‰, respectively (Yeung et al., 2017). This applies for any magmatic and crustal N_2, whether it is mantle-derived, inherited from the slab, or shallow crustal reservoirs (Labidi et al, 2020). In contrast, air has a pronounced disequilibrium $^{15}N^{15}N$ enrichment, leading to an atmospheric Δ_{30} value of 19.1±0.3‰ (2σ) (Yeung et al., 2017). We make use of this disequilibrium as a tracer for air contributions in natural fluids and identify the compositions of mantle sources for N_2 and light noble gases for 15 fumaroles and gases bubbling from springs in Costa Rica, Panama, Nicaragua, and El Salvador. Our $^{15}N^{15}N$ data allows determination of the $N_2/{}^3He$, $^3He/{}^{36}Ar$ and $^3He/{}^{22}Ne$ ratios for the CAVA mantle sources. Using an updated ^3He outgassing flux for the region, we provide a new range of estimates for the N_2 outgassing flux along the Central American arc. Our result has implications for the net subduction flux of nitrogen, suggesting that the net sequestration of nitrogen to the mantle is within error of zero.

2. Geological context and samples

The CAVA results from the eastward subduction of the Cocos Plate beneath the Caribbean Plate. Abundant literature describes the spectrum of sub-arc mantle sources, incorporating slab sedimentary components beneath Nicaragua, to volcanic seamounts derived from Galapagos underneath Costa Rica and Panama (Carr et al., 2003; Gazel et al., 2009; Hoernle et al., 2008; Patino et al., 2000; Ranero and von Huene, 2000; Schwarzenbach et al., 2016).

Eight gas samples from fumaroles were collected from Poás and Momotombo volcanoes during several field expeditions in the early to mid-2000's with gas chemistry and isotope data published in Zimmer et al. (2004), Elkins et al. (2006), De Leeuw et al., (2007) and Fischer et al. (2015). Fumaroles had outlet temperatures ranging from 98°C to 747°C. Samples were collected in pre-evacuated Giggenbach bottles filled with 5N NaOH solution (Giggenbach and Goguel, 1989). Gas splits were taken from the headspace of the bottles with sealed glass tubes shortly after sample collection and stored until analyzed for this work. Five gases from the Poás crater were collected between 2003 and 2006, from the fumarolic sites "Official" and "Naranja", at temperatures between 98°C and 158°C. For these, we report new N_2 isotopologue and $^{40}Ar/^{36}Ar$ data. $^{3}He/^{4}He$ of these samples are 7.0±0.2 R_A (Hilton et al., 2010) where R_A is air $^{3}He/^{4}He$ or 1.384 x 10^{-6}. Gas chemistry is available from previous work (Fischer et al., 2015). One fumarole sample was collected at Santa Ana Volcano (Salvador), with a vent temperature of 400°C. It has a helium isotope ratio of 7.5±0.1 R_A (De Leeuw et al., 2007). The He-Ne-Ar abundances are known (De Leeuw et al., 2007). No $^{40}Ar/^{36}Ar$ is available but other gases from El Salvador all have

141 near-atmospheric $^{40}Ar/^{36}Ar$ ratios (Snyder et al., 2003). We additionally discuss two
142 fumarole gas samples collected at Momotombo in Nicaragua, at an outlet temperature of
143 ~750°C. For these two samples, we report new $^{40}Ar/^{36}Ar$ isotope measurements. N_2
144 isotopologues, helium isotopes, He-Ne-Ar and major gas chemistry data for these samples
145 are available from previous work (Elkins et al., 2006; Yeung et al., 2017). Hot springs found
146 in the flanks of volcanic arcs are the most accessible samples, and hence are routinely used
147 to characterize volcanic endmembers (e.g. Snyder et al., 2003). As a means to compare
148 these to our fumaroles, we also report data from seven gases from bubbling springs in
149 Costa Rica and Panama, collected in 2018 as part of the *Biology Meets Subduction* initiative.
150 Sample collection sites are shown on figure 1. Samples were collected in 15 cm^3 copper
151 tubes following standard procedures. Waters in the springs had temperatures between
152 29°C and 55°C. For these, we report major element gas compositions, N_2 isotopologues and
153 He–Ne–Ar systematic data.

154 **3. Methods**

155 Gas aliquots were split up to three ways and processed for (1) gas chemistry, (2) N_2,
156 and (3) noble gases systematics. Inorganic gas components (such as N_2, He, Ar and O_2) and
157 methane were separated and quantified on a TCD gas chromatograph coupled with a
158 quadrupole mass spectrometer as in earlier work (Fischer et al., 2015). This allowed
159 determining the N_2/He and N_2/Ar ratios of each gas splits. Nitrogen isotopologues were
160 determined via high-resolution mass spectrometry at the University of California, Los
161 Angeles (Young et al., 2016). Noble gas analyses were conducted at the University of Oxford
162 (UK) and at the University of New Mexico using standard methods (Barry et al., 2016; Lee
163 et al., 2017). Details may be found in the supplementary online file.

4. Results

We present an integrated dataset that includes concentrations of He, Ne, Ar, N_2, O_2, and CH_4, elemental ratios of those gases, noble gas isotope compositions, and N_2 isotopologue ratios. Data for the fumaroles (n=8) are in table 1 and data for the springs (n=7) are in table 2.

4.1. $\delta^{15}N$ and Δ_{30} relationships

Newly determined Δ_{30} values vary between 19.3±0.4‰ and 3.5±1.0‰ (1σ uncertainty, Fig. 2). Two previously published data points from Momotombo extend the range down to 1.5±0.6‰ and are plotted on Fig. 2 (Yeung et al. 2017). The highest Δ_{30} is similar to the air value of 19.1±0.3‰ (2σ). The range in Δ_{30} values suggests samples incorporate variable amounts of atmospheric nitrogen, contributing between ~8 and ~100% of the total N_2. Fumaroles from Poás and Momotombo have the lowest Δ_{30} values, indicating that these fumaroles have the lowest air-derived N_2 contributions. A range of $\delta^{15}N$ values is observed, with values of between –3.7±0.3‰ and +4.2±0.3‰ (Fig. 2). For Poás and Momotombo, $\delta^{15}N$ values are +0.4±0.3‰ and +5.4±0.3‰ respectively, where air contributions are at their lowest values (minimum Δ_{30}). The $\delta^{15}N$ values as a whole (with both low and high Δ_{30}) are within the range of $\delta^{15}N$ values of between –3.0±0.6 and 6.3±0.3‰ (n=73) reported previously for central American gases (Elkins et al., 2006; Fischer et al., 2015, 2002; Snyder et al., 2003; Zimmer et al., 2004). The $\delta^{15}N$ values exhibit a negative correlation with Δ_{30} values (Fig. 2).

4.2. Noble gas isotopes

Concentrations of He, Ne and Ar vary over 4 orders of magnitude and are correlated (Table 1 and 2). We observe $^{40}Ar/^{36}Ar$ ratios between 297±5 and 342±5 for our samples (Table 1 and 2), far from the upper mantle value of ~ 25,000 (Moreira et al. 1998) but close to air at 298.5 (Lee et al., 2006). This is comparable to the known range of values for Central American rocks and gases of between 292±7 and 310±5 (Fischer et al., 2005; Kennedy et al., 1991; Snyder et al., 2003; Staudacher and Allègre, 1988). The $^{20}Ne/^{22}Ne$ and $^{21}Ne/^{22}Ne$ ratios are known only for the hot springs, and data appear indistinguishable from air (Table 2).

The $^{3}He/^{4}He$ ratios vary substantially, between 0.3 and 7.6±0.1 R_A. Unlike Ne and Ar, the He budget is not significantly affected by atmospheric components and instead reflect appreciable deep contributions. The $^{3}He/^{4}He$ ratios are broadly correlated with $^{4}He/^{20}Ne$ ratios (Fig. 3). Most of the data are explained by two-component mixing between air ($^{3}He/^{4}He$ =1 R_A by definition, $^{4}He/^{20}Ne$ =0.3188) and a magmatic endmember. The magmatic component has a $^{3}He/^{4}He$ of ~7 (Fig. 3). The $^{4}He/^{20}Ne$ ratio of the magmatic component must be at least as high as the highest value from our dataset, ~270. Three Costa Rican springs show a clear offset from the two-component mixing line, showing much lower $^{3}He/^{4}He$ ratios at a given $^{4}He/^{20}Ne$ value. Similar features in other Central American gases were interpreted to result from mixing with gases from crustal fluids (De Leeuw et al., 2007).

4.3. Nitrogen, oxygen and methane concentrations

Nitrogen concentrations vary from 0.2 vol% to 93 vol% in the springs, and from 0.6 vol% to 1.9 vol% in the fumaroles (Table 1 and 2). Oxygen concentrations are variable,

resulting in O_2/N_2 ratios ranging over two orders of magnitude, between 3.8 x 10^{-4} to 1.1 x 10^{-1} (Supplementary Fig. 1). The O_2/N_2 ratios are not directly correlated with Δ_{30} values (supplementary Fig. 1), suggesting that O_2/N_2 is not a reliable indicator of the presence of nitrogen from air. Methane concentrations are below 0.1 vol % for most samples, with the exception of two of the Costa Rica hot springs, where CH_4 concentrations are as high as ~80 vol %, suggesting contributions from shallow crustal gases (Snyder et al. 2003). N_2/CH_4 varies over 5 orders of magnitude, between ~1.2 x 10^{-1} to ~2.1 x 10^4, but remains uncorrelated with Δ_{30} values (Supplementary Fig. 1).

4.4. Nitrogen - noble gas ratios

We compute N_2/Ar, $N_2/^{36}Ar$, N_2/He and $N_2/^3He$ ratios, with a ±20% relative uncertainty on individual samples. N_2/Ar ratios are between 21 and 120 for most samples, with one sample from Momotombo at 507 (Fig. 4). For comparison, the air value is ~84, air-saturated water (ASW) at STP is ~41, and MORB gases have N_2/Ar ratios of 55±5 (Javoy and Pineau, 1991), although a higher estimate of ~120±40 (Marty and Dauphas, 2003) was derived from MORB samples with unusually radiogenic $^{40}Ar/^{36}Ar$ ratios (data from Marty et al., 1999). For samples where $^{40}Ar/^{36}Ar$ was measured, $N_2/^{36}Ar$ ratios vary between 1.2×10^4 and 4.2×10^4. Assuming the $^{40}Ar/^{36}Ar$ is atmospheric as for other Central American gas samples (Snyder et al., 2003), the $N_2/^{36}Ar$ range extends to between 6.5×10^3 and 1.5×10^5 (Fig. 4). This includes values below and above both air (2.5×10^4) and air-saturated water at STP (1.3×10^4). The highest $N_2/^{36}Ar$ value remains well below estimates of the convective mantle of ~ 2×10^6 (Labidi et al., 2020; Marty and Humbert, 1997) even for samples where Δ_{30} is low.

The N_2/He ratios vary between 1.5×10^2 and 4.2×10^4, below the value of air of 1.5×10^5 or air-saturated water $\sim 3.0 \times 10^5$ (Fig. 5). Similarly, $N_2/^3$He ratios vary between 1.6×10^7 and 1.1×10^{11} (Fig. 5), mostly below the value of air and ASW of 1.0×10^{11} and $\sim 2.0 \times 10^{11}$ respectively (Ballentine et al., 2002). The N_2/He (and $N_2/^3$He ratios) are correlated with Δ_{30} values and are described by two-component mixing hyperbolae between air (or air-saturated waters) and high-temperature components with elevated N_2/He (and $N_2/^3$He ratios) relative to MORB gases (Fig. 5).

4.5. Noble gas ratios

The ^{3}He/^{22}Ne ratios range over 4 orders of magnitude, between 8.9×10^{-6} and 2.7×10^{-2} (Fig. 6). These values are between air, at 4.5×10^{-6}, and upper-mantle gases at $\sim 5.5 \times 10^1$ (Moreira et al., 1998). The ^{4}He/^{20}Ne ratios are also ranging between air and the upper-mantle value (Supplementary Figure 2). ^{3}He/^{22}Ne (and ^{4}He/^{20}Ne) ratios are correlated with Δ_{30} values (Fig. 6, Supp Fig. 2). At Δ_{30} = 0 the high-temperature component appears to have He/Ne ratios lower than MORB gases by about four orders of magnitude (Fig. 6, Supp Fig. 2). The ^{3}He/^{36}Ar ratio ranges between 1.6×10^{-6} and 1.7×10^{-4} (Fig. 6). This is higher than the air value of 2.5×10^{-7}, but considerably lower than the upper-mantle value of $\sim 5.0 \times 10^{-1}$ (Moreira et al., 1998; Raquin et al., 2008). A similar observation can be made of the ^{4}He/^{40}Ar ratio (Supp Fig. 2). The variations in ^{3}He/^{36}Ar (and ^{4}He/^{40}Ar) ratios are correlated with Δ_{30} values and at Δ_{30} =0, the high-T component shows ^{3}He/^{36}Ar ratios lower than MORB gases by about three orders of magnitude (Fig. 6, Supp Fig. 2). Most ^{22}Ne/^{36}Ar ratios in fumaroles and springs range between 1.3×10^{-1} and 3.1×10^{-3} (with one outlier at $\sim 6.5 \times 10^{-1}$, the Poás gas with the Δ_{30} value closest to air). The higher values are similar to the air and MORB values of 5.0×10^{-2} and 1.0×10^{-1},

255 respectively (Mukhopadhyay, 2012) and are observed for samples with air-like Δ_{30} values.
256 At Δ_{30} = 0, much lower $^{22}Ne/^{36}Ar$ values are observed, lower than both MORB and air by
257 one to two orders of magnitude (Table 1 and 2).
258
259 **5. Discussion**
260 Our rationale is that correlations between Δ_{30} and various isotope and element ratios
261 can be used to identify and correct for air components and reveal pristine high-
262 temperature endmembers. Air is identified with a Δ_{30} of 19.1±0.3‰, while any N_2
263 produced by a geologic process such as magmatic degassing has $\Delta_{30} \sim 0$ ‰ (Labidi et al.,
264 2020). Arguments against re-ordering and crustal contamination are given in the
265 supplementary discussion.
266
267 **5.1 Atmospheric N_2 may easily go unnoticed**
268 CAVA gas Δ_{30} values are variable, indicating commensurately variable contributions of
269 air to the N_2 budgets in hydrothermal discharges. Based on Δ_{30} data, air accounts for 40 to
270 100% of the N_2 in the springs. In fumaroles, air accounts for 8 to 90% of the N_2.
271 Atmospheric N_2 is therefore ubiquitous. Systematics involving $\delta^{15}N$, $[O_2]$, O_2/N_2, N_2/He and
272 N_2/Ar ratios may disentangle magmatic N_2 from air-derived N_2 in gas discharges (Sano et
273 al., 2001, Fischer et al. 2002, Elkins et al., 2006). The rationale for all of those approaches is
274 that air has known $\delta^{15}N$, O_2/N_2, N_2/He and N_2/Ar ratios, that are different from magmatic
275 components. Our Δ_{30} data present a series of challenges to these previous approaches. For
276 example, samples with high $^4He/^{20}Ne$ ratios were suggested to illustrate a volatile budget
277 largely uncontaminated by air, especially when a number of other criteria are met, e.g.,

O_2/N_2 ratios < 10^{-3}, high outlet temperatures, or non-atmospheric N_2/Ar ratios (Elkins et al., 2006). The Santa Ana volcano fumarole is vented at 400°C, a $^4He/^{20}Ne$ ~ 200 times higher than air and a O_2/N_2 ratio of ~10^{-4} (Table 1, Fig. 3), which would suggest minimal air contamination. However, the near-air Δ_{30} of 15.5±0.3‰ requires that ~80% of N_2 is from air in this sample, showing that high $^4He/^{20}Ne$, even in conjunction with high vent temperature and low O_2/N_2, is not necessarily sufficient evidence that N_2 is dominantly magmatic (See supplementary discussion).

5.2 **Atmospheric N_2 undergoes isotopic fractionation in hydrothermal systems**

Nitrogen isotope ratios could be a direct tracer of atmospheric N_2, since air and magma-derived nitrogen are thought to have distinct $\delta^{15}N$ values (Fischer et al., 2002, Sano et al., 2001). The Δ_{30} data confirm the veracity of this approach for most, but not all, samples. Gases (except those from Poás) fall on a single two-component mixing trend between air and a high-temperature component with near-zero Δ_{30} and $\delta^{15}N$ of ~ 5‰ (Fig. 2). For those, the air component appears unfractionated with respect to $\delta^{15}N$. When mixed with high-temperature volatiles, $\delta^{15}N$ increases and Δ_{30} values decrease (Fig. 2).

Samples from Poás are different. They form a unique linear mixing trend where both air-derived and high-temperature N_2 are distinct from elsewhere in the arc system, with $\delta^{15}N$ endmember values of –4.0±0.3‰ and +1.0±0.3‰ for air and the high-T component, respectively (Fig. 2). This represents a ~4‰ shift for both endmembers compared to values observed elsewhere on the arc. Our observation creates ambiguities at Poás, since there, and there only: (1) high-temperature $\delta^{15}N$ is only marginally higher than air; and (2)

301 air-derived N_2 has a $\delta^{15}N$ very similar to the MORB value of −5±2‰ (Javoy and Pineau,
302 1991, Marty et al., 1999).

303 The data from Poás require that atmospheric N_2 experienced a ~4‰ mass-dependent
304 $^{15}N/^{14}N$ fractionation in the sub-surface. This may result from the degassing of once air-
305 saturated waters. The isotopic fractionation associated with N_2 dissolved in water was
306 experimentally documented to be +0.9 to -0.4 ‰ from 6 to 60 °C (Lee et al., 2015). The
307 dissolved-gas isotope fractionation was shown to cross over at about 40 °C, from a positive
308 to a negative sign (Lee et al., 2015). Above 40 °C, the isotopic difference between dissolved
309 and gaseous N_2 increases: isotopically light N_2 is increasingly partitioned in the dissolved
310 fraction as temperature increases. This behavior indicates that a kinetic isotope effect
311 attends N_2 dissolution/degassing in geothermal waters (Lee et al., 2015). Using the
312 experimental results of Lee et al., (2015), we calculate the consequences of N isotope
313 fractionation during open-system degassing using Rayleigh fractionation. At 60 °C, with a
314 gas/dissolved-gas $^{15}N/^{14}N$ fractionation factor of 1.0004, the lowest $\delta^{15}N$ values of ~ −3.5
315 ‰ with air-like Δ_{30} require that the N_2 sampled by the fumaroles is the residuum left over
316 after degassing of about 99.98 % of the dissolved nitrogen. Extrapolating the temperature
317 dependence of the fractionation factor to 100 °C, 97% degassing of N_2 is required to
318 account for a $\delta^{15}N$ of ~ −3.5 ‰.

319 We envision the hydrothermal degassing to be the natural consequence of
320 hydrothermal systems experiencing continuous degassing in the absence of continuous
321 meteoric (air-saturated) water recharge. It is puzzling however that among the sites we
322 sampled, air nitrogen undergoes isotopic fractionation only at Poás. In order to explain this
323 observation, we suggest a restricted set of conditions is met in the Poás subsurface, but not

elsewhere. Gases from Momotombo and Santa Ana are vented at temperatures between 747 °C and 400 °C, respectively. No liquid water remains stable at those temperatures. Thus, isotope partitioning between water and gas is not occurring, and N_2 remains unfractionated. Spring gases are vented at temperatures between 29 °C and 59 °C (Table 2), at temperatures where degassing is probably limited. In contrast, at Poás, the fumaroles are vented at ~100-150 °C (Fischer et al., 2015). At these temperatures, liquid and gaseous water are stable and water/gas partitioning can occur. These conditions are comparable to those observed for hydrothermal gases from Iceland or Yellowstone, where negative $\delta^{15}N$ values were previously observed in conjunction with air like Δ_{30} values (Labidi et al., 2020). Our conclusion is also consistent with the observation of sporadically negative $\delta^{15}N$ (with no available Δ_{30} data) in Poás fumaroles sampled in 2001. Values as low as ~ –3.0‰ were observed in fumarole vented at temperature between 76 and 108 °C (Fischer et al., 2002). In other fumaroles (89-101 °C) sampled between 1998 and 2001, while unfractionated air-like $\delta^{15}N$ and N_2/Ar values were reported (Vaselli et al., 2003). More work is warranted to follow the potential Δ_{30}-$\delta^{15}N$ evolution of a given fumarole through time, but in the interim, we suggest caution in interpreting $\delta^{15}N$ data at Poás in the absence of Δ_{30}.

5.3. Is high-temperature nitrogen also fractionated?

Whether high-temperature components with Δ_{30} ~0‰ also experience $\delta^{15}N$ isotope fractionation in hydrothermal systems is an open question. At Momotombo, fumaroles have a high-temperature endmember with $\delta^{15}N$ ~+5‰ (Fig. 2.). There, vent temperatures are > 700 °C. This precludes liquid water to exist even at depths, ruling out the possibility of any water/gas isotope exchange. This is consistent with a previous observation of

unfractionated $\delta^{15}N$ for fumaroles when they are vented at > 300 °C (Fischer et al., 2005). At Poás however, the interpretation is not as straightforward, where the high-temperature endmember has a $\delta^{15}N$ ~+1‰ (Fig. 2), which is lower than at Momotombo by ~4‰, implying that a fractionation similar to that for the air component could have occurred. It is conceivable that high-T volatiles have been delivered to the water table *prior to* hydrothermal degassing, where they would experience $^{15}N/^{14}N$ fractionation together with the air-derived gases. In this interpretation, the high-T $\delta^{15}N$ value of ~+1‰ obtained by extrapolation to $\Delta_{30} = 0$ would not record the actual magmatic $\delta^{15}N$ value at Poás, and the Poás trend would be parallel to the main array as the result of a fractionation equally affecting both the atmospheric and high-T volatiles. However, with our dataset alone, we cannot exclude that high-T volatiles had been delivered to the fumaroles *after* hydrothermal degassing. If so, the Poás high-T endmember could be truly unique in $\delta^{15}N$, and the Poás trend being parallel to the main array (Fig. 2) would be fortuitous. This latter scenario relies on a coincidence, and thus appears unlikely, although it cannot be fully ruled out.

5.4. N_2/Ar ratios place independent constraints on hydrothermal degassing

The solubilities of argon and nitrogen are distinct by about a factor of 2 in geothermal waters at temperatures between 20 and 100 °C (Ballentine et al, 2002). Thus, water/gas processes may be tracked with N_2/Ar ratios, independently of nitrogen isotopes. Low N_2/Ar ratios for air-like Δ_{30} values are observed at Poás, while most other samples have near-air values for N_2/Ar at air-like Δ_{30} (Fig. 4), confirming that at Poás liquid-gas

partitioning occurred in the sub-surface. We can again use a Rayleigh fractionation calculation to infer the amount of degassing implied by the N_2/Ar ratio data, where

$$N_2/Ar = (N_2/Ar)_0 f^{\alpha-1} \quad (1)$$

and

$$\alpha = (K_{N_2}/K_{Ar}), \quad (2)$$

where f is the fraction of remaining Ar in the water, $(N_2/Ar)_0$ the known starting composition of ASW, and α is the fractionation coefficient given for a gas/liquid system given by Equation (2), and K_i is the Henry's-law constant for species i, as compiled in Ballentine et al., (2002). Taking $(N_2/Ar)_0$ to be 41, we find that the lowest N_2/Ar value of ~ 10 implied by our data occurs for about 94% degassing of N_2 (75% degassing of Ar) prior to sampling (Fig. 4). To first order, this degree of degassing is consistent with estimates made on the basis of $^{15}N/^{14}N$ values (section 5.2).

There is a caveat to this interpretation. Data for $\delta^{15}N$ and N_2/Ar appear consistent with fractionation within hydrothermal systems, but no direct correlation is observed between $\delta^{15}N$ and N_2/Ar (Table 1). This is perhaps because degassing may yield variable $^{15}N/^{14}N$ and N_2/Ar fractionations depending on the exact temperature and pressure conditions (Lee et al., 2015; Warr et al., 2015). Under conditions making the gas behavior non-ideal, degassing may change the N_2-Ar solubility relationship, as suggested for heavier noble gases (Labidi et al., 2020, Warr et al., 2015). Additionally, small contributions of high-temperature volatiles are likely to cause shifts in $\delta^{15}N$ with no obvious increases in N_2/Ar ratios (Fig. 4). This is because high-temperature endmembers with Δ_{30} = 0‰ appear to have N_2/Ar and $N_2/^{36}Ar$ ratios of ~ 100 and ~ 10^4, respectively (Fig. 4). These values are

essentially similar to air, consistent with pioneer work on the CAVA (Hilton et al., 2002; Snyder et al., 2003), but remain lower than volcanic endmembers at other arcs (Taran, 2009; Zelenski and Taran, 2011). We note that one of the Momotombo fumaroles has a high N_2/Ar of ~500, higher than other high-temperature gases by a factor of 5. The significance of variable N_2/Ar ratios in Central American high-temperature endmembers must be systematically investigated in future work, with Δ_{30} data.

5.5. δ^{15}N-N_2/He relationships constrained by Δ_{30} data

In contrast to argon, the solubility of helium in geothermal waters is nearly indistinguishable from that of nitrogen in the relevant temperature range (Ballentine et al., 2002). Data can be accounted for by mixing between air and an endmember with $N_2/^3$He ratios ~ 10^8 (Fig. 5). This is higher than MORB gases that are characterized by $N_2/^3$He ratios of about 10^6 (Javoy and Pineau, 1991, Marty and Humbert, 1999). The Poás fumaroles involve a mixing scenario that is similar to the one for Momotombo, involving high-T endmembers with a $N_2/^3$He of ~10^8 (Fig. 5). This observation argues against a significant contribution of MORB derived volatiles to Poás volcanic gas discharges. Overall light δ^{15}N values from Poás were previously suggested to reflect a contribution from MORB-derived volatiles, contrary to the majority of other CAVA gas discharges that showed predominantly slab-derived N (Fischer et al., 2002, Elkins et al., 2006). Our new Δ_{30} data suggest a revision to the interpretation of ^{15}N depletions and show that they rather reflect contributions of fractionated air (Fig. 2) mixed with a predominantly non-MORB magmatic component with elevated N_2/He ratios (Fig. 5).

5.6. Magmatic endmembers throughout the arc are enriched in N_2

In an attempt to characterize subduction volatiles, we constrain the high-temperature endmembers for nitrogen isotopes and N_2/Ar, N_2/He, He/Ne and He/Ar ratios. Endmember compositions are calculated assuming two-component mixing with air constrained by Δ_{30} values, as described above. We focus on fumarole data to constrain endmember compositions, since they show the lowest Δ_{30} and no evidence of crustal contamination (see supplementary discussion).

The derived N_2/He ratios are higher than MORB by two orders of magnitude. In contrast, He/Ne, He/Ar and $N_2/^{36}$Ar are all lower than MORB by two to three orders of magnitude (Fig. 4-6). The simplest explanation is that slab-derived N_2, Ne and Ar were added to a depleted mantle source with an unmodified helium signature (Fig. 7). A straightforward quantification of slab-derived N_2, Ar and Ne to the mantle wedge is possible using $N_2/^3$He, ^{3}He/^{22}Ne and ^{3}He/^{36}Ar ratios. This approach is viable if ^{3}He subduction is negligible (Staudacher and Allegre, 1988), notwithstanding that slab components are required to contribute minute ^{4}He ingrowth from subducted uranium (Hilton et al., 2002).

The high-T, arc magma endmembers at Poás and Momotombo have $N_2/^3$He ratios two orders of magnitude higher than MORB, requiring nitrogen addition to mantle sources in these arc systems. Sedimentary nitrogen may be a straightforward contributor to the Momotombo source, explaining the high δ^{15}N of + 5‰ there (Fig. 7). Sediments on the modern oceanic crust directly offshore of Central America are likely candidates, since they have an average δ^{15}N of ~5‰ (Li and Bebout, 2005). Poás volcano is more complicated, because the lower δ^{15}N (Fig. 2) may not be a genuine representation of the Poás mantle

source. We note that because $N_2/^3He$ are indistinguishable between Poás and Momotombo, they must have received a comparable amount of slab-derived N.

Sub-arc magmatic endmembers have lower $^3He/^{22}Ne$ and $^3He/^{36}Ar$ ratios by 2 to 3 orders of magnitude compared to those of MORBs. Like nitrogen, this likely requires substantial addition of slab-derived neon and argon to a mantle source. Samples with near-zero Δ_{30} have $^{22}Ne/^{36}Ar$ lower than both MORB and air by one to two orders of magnitude (Table 1), with values trending toward $\sim 0.7 \times 10^{-2}$. This is similar to the median ratio of an entire section of altered oceanic crust and sediments of $\sim 1 \times 10^{-2}$ (Chavrit et al., 2016). The similarity in $^{22}Ne/^{36}Ar$ between the magmatic endmembers at CAVA and the slab is consistent with a mantle wedge being overwhelmed by the addition of slab-derived neon and argon. Samples with near-zero Δ_{30} also have atmospheric $^{40}Ar/^{36}Ar$ values (Table 1), indicating that Ar from the mantle wedge has retained the noble gas isotopic signature of its subducted atmospheric source. This is likely explained by the contribution of surface-derived argon with atmospheric $^{40}Ar/^{36}Ar$ ratios to the mantle wedge. This sheds new light on atmospheric $^{40}Ar/^{36}Ar$ observed systematically in all known Central American fumaroles (Snyder et al. 2003) and essentially all gas discharges sampled to date from subduction zones (Hilton et al., 2002, Sano and Fischer, 2013): A likely origin for the atmospheric Ar in high-T endmembers is devolatilizing subducted protoliths that are otherwise known to have atmospheric Ar isotopic signatures (Chavrit et al., 2016; Holland and Ballentine, 2006; Staudacher and Allègre, 1988). Our high-T data shows that not all of the subducted air-derived Ar is transferred into the deeper mantle and that some of it is released via arc volcanism. Our data also dispels the notion that atmospheric Ar-isotope

459 signatures of arc-gases are exclusively the result of shallow atmospheric contamination in
460 the hydrothermal system.
461
462 **5.7 Revisiting volatile fluxes in the central American subduction zone.**
463 The perspective that volatiles from the mantle wedge incorporate recycled argon is
464 problematic, as it limits the use of nitrogen excesses, N_2^*, calculated on the basis of N_2/Ar
465 ratios (Fischer et al. 1998,2002, Hilton et al., 2002). We show here that magmatic volatiles
466 deliver measurable amounts of argon (with atmospheric $^{40}Ar/^{36}Ar$) to the fumaroles.
467 Consequently, assumptions on N_2^* may naturally underestimates the outgassing flux of N_2.
468 Estimates for the fluxes of N_2, Ar, and Ne can be obtained from ^3He degassing fluxes. Using a
469 combination of S/CO_2, He/CO_2 and $^3He/^4He$ ratios, and an SO_2 flux of 21.3 x 10^9 mol/yr,
470 Hilton et al. (2002) derived a ^3He flux of 5.4 mol/yr for the entire CAVA. Using the CAVA
471 CO_2 flux from Fischer et al., (2019) of 94 x 10^9 mol/yr, and a $CO_2/^3He$ ratio of 2 x 10^{10}
472 (Kagoshima et al., 2015), we obtain a ^3He flux 4.7 mol/yr. Here, we take a ^3He flux of 5.0
473 mol/yr for the sake of illustration. We combine our new elemental ratios estimates for the
474 CAVA source (Fig. 4-6) with ^3He fluxes to derive new estimates for N_2, ^{36}Ar, and ^{22}Ne
475 outgassing fluxes in the central American arc.
476 We derive $N_2/^3He$ ratios between 8 x 10^7 and 2 x 10^8 for magmatic volatiles in Central
477 America (Fig. 5), from samples with Δ_{30} < 5‰. This results in a N_2 flux between 4.0 x 10^8
478 and 1.0 x10^9 mol N_2/y (or 1.1 x 10^{10} and 2.8 x 10^{10} g N/ y). This range for the nitrogen mass
479 flux is higher than previous estimates of 8.2 x 10^9 g N/ y (Fischer et al., 2002, Hilton et al.,
480 2002). Our derived range of nitrogen fluxes overlaps the estimated flux of subducting
481 nitrogen of 1.6 x 10^{10} g N/ y (1.1 x 10^9 mol N/y, or 5.7 x 10^8 mol N_2/yr), given with no

uncertainty in Busigny et al. (2019) and Li and Bebout (2005). This suggests that in the Central American subduction zone, the N_2 cycle is not required to be out of equilibrium. Instead, the revisited fluxes being identical within uncertainty, they allow N_2 to be quantitatively recycled through the mantle wedge and returned to the surface by degassing rather than being delivered to the deep mantle. An additional source of outgassing underestimation, here, is that we ignore forearc devolatilization for N_2, known to occur in the CAVA (Inguaggiato et al., 2004). Future work will be necessary to constrain this fraction of the N_2 flux that will inevitably increase the outgassing flux further. In any case, our newly defined N_2 outgassing fluxes are high, and in the range of subducting fluxes. Because this subduction zone is relatively "warm" and therefore more similar to subduction zones in the past over geological timescales (Keller and Schoene, 2018; Martin and Moyen, 2002), the finding that nitrogen is recycled by subduction and arc magmatism in the Central American system suggests that nitrogen subduction could have been inefficient through geological time. This conclusion is also in agreement with recent experimental work suggesting warm subduction zones limit nitrogen recycling in the deep mantle (Jackson et al., 2021).

We estimate the $^3He/^{36}Ar$ of magmatic inputs to be $\sim 10^{-4}$ (Fig. 6). A $^3He/^{36}Ar$ ratio of $\sim 10^{-4}$ leads to a degassing ^{36}Ar flux of $\sim 5.0 \times 10^4$ mol/y (1.8×10^6 g ^{36}Ar/y) in Central America. Using 1.4×10^{16} g of subducted crust, depths of ~6 km of oceanic crust and ~500 m of sediments, and the noble gases abundances in the oceanic crust (Chavrit et al., 2016), we derive a ^{36}Ar subduction flux of 1.1×10^8 cm^3 STP/y, or 4.5×10^4 mol ^{36}Ar/y. Because of the large uncertainties in ^{36}Ar concentrations in rocks (Chavrit et al., 2016), this subduction flux estimate is probably associated with a ~50% uncertainty, and is presented here for illustration only. We note however that subduction and outgassing ^{36}Ar flux compare

favorably. Like nitrogen, our flux analysis seems to allow quantitative release of slab-derived ^{36}Ar to the mantle wedge, which would not require substantial ^{36}Ar recycling into the deep mantle in this subduction zone. The same conclusion holds for neon. Using a $^{3}He/^{22}Ne$ of ~2 x 10^{-2} (Fig. 6), we obtain a ^{22}Ne degassing flux of ~2.5 x 10^{2} mol/y (5.5 x 10^{3} g ^{22}Ne/y). The $^{22}Ne/^{36}Ar$ of subducting components is largely variable, around a mode of ~10^{-2} (Chavrit et al., 2016). This yields a ^{22}Ne subduction flux of 1.1 x 10^{6} cm^{3} STP/y, or 4.5 x 10^{2} mol ^{22}Ne/y. Again, although large uncertainties must be taken into consideration, the neon subduction and degassing fluxes appear equivalent, arguing in favor of quantitative ^{22}Ne recycling in the central American subduction zone back to the surface.

The simplest interpretation of the fluxes derived here is that the Central American subduction zone acts as a subduction barrier for N, Ar, and Ne: volcanic fluxes for N_2, Ar, and Ne, determined with the $^{15}N^{15}N$ approach, *no longer require* subduction of these elements past the sub-arc melting region in the central American subduction zone.

6. Conclusion

Gas discharges in Central America are volatile mixtures involving contributions from at least three endmembers: air (±fractionated air), crust, and mantle-derived components. Using Δ_{30} as a tracer of nitrogen from air in fumaroles and springs, we show that O_2/N_2 ratios are unreliable tracers of air in these systems. We also show that $\delta^{15}N$ and N_2/Ar ratios experienced fractionation during water degassing at depth, rendering these unreliable as signatures of air where liquid water is thermodynamically stable. This is problematic since the degassing fractionation may lead to $\delta^{15}N$ values that insidiously

mimic MORB gases. This does not seem to affect magmatic components, but more work is needed on Poás – where interaction with the hydrothermal system may be significant, before a firm conclusion can be reached. A preliminary conclusion is that without Δ_{30} data, the $\delta^{15}N$-N_2-Ar systematics may be deceptive, and can lead to confusion with regard to the origin of N_2 in mixed gases.

We derive estimates of N_2/He, He/Ar and He/Ne ratios that reliably exclude atmospheric components. N_2, Ar and Ne enrichments by two or three orders of magnitude compared to a MORB source are observed. They are attributed to mantle wedge sources incorporating slab-derived gases. Using known ^{3}He degassing fluxes, we calculated N_2, Ne and Ar degassing fluxes for the Central American arc that could balance subduction fluxes, within uncertainties, no longer requiring the Central American arc to have heavily imbalanced volatile cycles.

Acknowledgement

This study was supported by the Deep Carbon Observatory through Sloan Foundation grant numbers G-2018-11346 to EDY. This work was also supported by grant G-2016-7206 from the Alfred P. Sloan Foundation and the Deep Carbon Observatory to PHB. Karen Lloyd and Donato Giovannelli are thanked for co-organizing the Subduction meets Biology initiative. Further, we acknowledge the National Science Foundation (NSF) award MGG-2015789 to PHB. We thank Yuri Taran and an anonymous reviewer for constructive and helpful comments. Rosemary Hickey-Vargas is thanked for editorial handling.

References

Barry, P.H., Lawson, M., Meurer, W.P., Warr, O., Mabry, J.C., Byrne, D.J., Ballentine, C.J., 2016. Noble gases solubility models of hydrocarbon charge mechanism in the Sleipner Vest gas field. Geochim. Cosmochim. Acta 194, 291–309.

Bebout, G.E., Agard, P., Kobayashi, K., Moriguti, T., Nakamura, E., 2013. Devolatilization history and trace element mobility in deeply subducted sedimentary rocks: Evidence from Western Alps HP/UHP suites. Chem. Geol. 342, 1–20.

Bekaert, D.V., Turner, S.J., Broadley, M.W., Barnes, J.D., Halldórsson, S.A., Labidi, J., Wade, J., Walowski, K.J., Barry, P.H., 2020. Subduction-Driven Volatile Recycling: A Global Mass Balance. Annu. Rev. Earth Planet. Sci. 49.

Busigny, V., Cartigny, P., Laverne, C., Teagle, D., Bonifacie, M., Agrinier, P., 2019. A re-assessment of the nitrogen geochemical behavior in upper oceanic crust from Hole 504B: Implications for subduction budget in Central America. Earth Planet. Sci. Lett. 525, 115735.

Busigny, V., Cartigny, P., Philippot, P., Ader, M., Javoy, M., 2003. Massive recycling of nitrogen and other fluid-mobile elements (K, Rb, Cs, H) in a cold slab environment: evidence from HP to UHP oceanic metasediments of the Schistes Lustrés nappe (western Alps, Europe). Earth Planet. Sci. Lett. 215, 27–42. https://doi.org/10.1016/s0012-821x(03)00453-9

Carr, M.J., Feigenson, M.D., Patino, L.C., Walker, J.A., 2003. Volcanism and geochemistry in Central America: Progress and problems. Geophys. Monogr. Geophys. Union 138, 153–174.

Chavrit, D., Burgess, R., Sumino, H., Teagle, D.A.H., Droop, G., Shimizu, A., Ballentine, C.J., 2016. The contribution of hydrothermally altered ocean crust to the mantle halogen and noble gas cycles. Geochim. Cosmochim. Acta 183, 106–124.

De Leeuw, G.A.M., Hilton, D.R., Fischer, T.P., Walker, J.A., 2007. The He–CO2 isotope and relative abundance characteristics of geothermal fluids in el salvador and honduras: New constraints on volatile mass balance of the central american volcanic arc. Earth Planet. Sci. Lett. 258, 132–146.

Elkins, L.J., Fischer, T.P., Hilton, D.R., Sharp, Z.D., McKnight, S., Walker, J., 2006. Tracing nitrogen in volcanic and geothermal volatiles from the Nicaraguan volcanic front. Geochim. Cosmochim. Acta 70, 5215–5235.

Fischer, T.P., Hilton, D.R., Zimmer, M.M., Shaw, A.M., Sharp, Z.D., Walker, J.A., 2002. Subduction and recycling of nitrogen along the Central American margin. Science (80-.). 297, 1154–1157.

Fischer, T.P., Ramírez, C., Mora-Amador, R.A., Hilton, D.R., Barnes, J.D., Sharp, Z.D., Le Brun, M., de Moor, J.M., Barry, P.H., Füri, E., Shaw, A.M., 2015. Temporal variations in fumarole gas chemistry at Poás volcano, Costa Rica. J. Volcanol. Geotherm. Res. 294, 56–70. https://doi.org/10.1016/j.jvolgeores.2015.02.002

581 Fischer, T.P., Takahata, N., Sano, Y., Sumino, H., Hilton, D.R., 2005. Nitrogen isotopes of the mantle: Insights from mineral
582 separates. Geophys. Res. Lett. 32.
583 Gazel, E., Carr, M.J., Hoernle, K., Feigenson, M.D., Szymanski, D., Hauff, F., Van Den Bogaard, P., 2009. Galapagos-OIB
584 signature in southern Central America: Mantle refertilization by arc–hot spot interaction. Geochemistry, Geophys.
585 Geosystems 10.
586 Hilton, D.R., Fischer, T.P., Marty, B., 2002. Noble gases and volatile recycling at subduction zones. Rev. Mineral.
587 geochemistry 47, 319–370.
588 Hilton, D.R., Ramirez, C.J., Mora-Amador, R., Fischer, T.P., Füri, E., Barry, P.H., Shaw, A.M., 2010. Monitoring of temporal and
589 spatial variations in fumarole helium and carbon dioxide characteristics at Poás and Turrialba volcanoes, Costa Rica
590 (2001-2009). Geochem. J. 44, 431–440.
591 Hoernle, K., Abt, D.L., Fischer, K.M., Nichols, H., Hauff, F., Abers, G.A., Van Den Bogaard, P., Heydolph, K., Alvarado, G., Protti,
592 M., 2008. Arc-parallel flow in the mantle wedge beneath Costa Rica and Nicaragua. Nature 451, 1094–1097.
593 Holland, G., Ballentine, C.J., 2006. Seawater subduction controls the heavy noble gas composition of the mantle. Nature
594 441, 186–191. https://doi.org/10.1038/nature04761
595 Inguaggiato, S., Taran, Y., Grassa, F., Capasso, G., Favara, R., Varley, N., Faber, E., 2004. Nitrogen isotopes in thermal fluids
596 of a forearc region (Jalisco Block, Mexico): Evidence for heavy nitrogen from continental crust. Geochemistry,
597 Geophys. Geosystems 5.
598 Jackson, C.R.M., Cottrell, E., Andrews, B., 2021. Warm and oxidizing slabs limit ingassing efficiency of nitrogen to the
599 mantle. Earth Planet. Sci. Lett. 553, 116615.
600 Javoy, M., Pineau, F., 1991. The volatiles record of a "popping" rock from the Mid-Atlantic Ridge at 14°N: chemical and
601 isotopic composition of gas trapped in the vesicles. Earth Planet. Sci. Lett. 107, 598–611.
602 Keller, B., Schoene, B., 2018. Plate tectonics and continental basaltic geochemistry throughout Earth history. Earth Planet.
603 Sci. Lett. 481, 290–304.
604 Kennedy, B.M., Hiyagon, H., Reynolds, J.H., 1991. Noble gases from Honduras geothermal sites. J. Volcanol. Geotherm. Res.
605 45, 29–39.
606 Labidi, J., Barry, P.H., Bekaert, D. V, Broadley, M.W., Marty, B., Giunta, T., Warr, O., Lollar, B.S., Fischer, T.P., Avice, G., 2020.
607 Hydrothermal 15 N 15 N abundances constrain the origins of mantle nitrogen. Nature 580, 367–371.
608 Lee, H., Fischer, T.P., Muirhead, J.D., Ebinger, C.J., Kattenhorn, S.A., Sharp, Z.D., Kianji, G., Takahata, N., Sano, Y., 2017.
609 Incipient rifting accompanied by the release of subcontinental lithospheric mantle volatiles in the Magadi and
610 Natron basin, East Africa. J. Volcanol. Geotherm. Res. 346, 118–133.
611 Lee, H., Sharp, Z.D., Fischer, T.P., 2015. Kinetic nitrogen isotope fractionation between air and dissolved N2 in water:

612 Implications for hydrothermal systems. Geochem. J. 49, 571–573.
613 Lee, J.-Y., Marti, K., Severinghaus, J.P., Kawamura, K., Yoo, H.-S., Lee, J.B., Kim, J.S., 2006. A redetermination of the isotopic
614 abundances of atmospheric Ar. Geochim. Cosmochim. Acta 70, 4507–4512.
615 Li, L., Bebout, G.E., 2005. Carbon and nitrogen geochemistry of sediments in the Central American convergent margin:
616 Insights regarding subduction input fluxes, diagenesis, and paleoproductivity. J. Geophys. Res. Solid Earth 110.
617 Libourel, G., Marty, B., Humbert, F., 2003. Nitrogen solubility in basaltic melt. Part I. Effect of oxygen fugacity. Geochim.
618 Cosmochim. Acta 67, 4123–4135. https://doi.org/10.1016/s0016-7037(03)00259-x
619 Martin, H., Moyen, J.-F., 2002. Secular changes in tonalite-trondhjemite-granodiorite composition as markers of the
620 progressive cooling of Earth. Geology 30, 319–322.
621 Marty, B., Humbert, F., 1997. Nitrogen and argon isotopes in oceanic basalts. Earth Planet. Sci. Lett. 152, 101–112.
622 Mikhail, S., Sverjensky, D.A., 2014. Nitrogen speciation in upper mantle fluids and the origin of Earth's nitrogen-rich
623 atmosphere. Nat. Geosci. 7, 816–819. https://doi.org/10.1038/ngeo2271
624 http://www.nature.com/ngeo/journal/v7/n11/abs/ngeo2271.html#supplementary-information
625 Moreira, M., Kunz, J., Allegre, C., 1998. Rare gas systematics in popping rock: isotopic and elemental compositions in the
626 upper mantle. Science (80-.). 279, 1178–1181.
627 Mukhopadhyay, S., 2012. Early differentiation and volatile accretion recorded in deep-mantle neon and xenon. Nature
628 486, 101–104. https://doi.org/10.1038/nature11141
629 Patino, L.C., Carr, M.J., Feigenson, M.D., 2000. Local and regional variations in Central American arc lavas controlled by
630 variations in subducted sediment input. Contrib. to Mineral. Petrol. 138, 265–283.
631 Peacock, S.M., van Keken, P.E., Holloway, S.D., Hacker, B.R., Abers, G.A., Fergason, R.L., 2005. Thermal structure of the Costa
632 Rica–Nicaragua subduction zone. Phys. Earth Planet. Inter. 149, 187–200.
633 Plank, T., Kelley, K.A., Zimmer, M.M., Hauri, E.H., Wallace, P.J., 2013. Why do mafic arc magmas contain~ 4 wt% water on
634 average? Earth Planet. Sci. Lett. 364, 168–179.
635 Ranero, C.R., von Huene, R., 2000. Subduction erosion along the Middle America convergent margin. Nature 404, 748–752.
636 Raquin, A., Moreira, M.A., Guillon, F., 2008. He, Ne and Ar systematics in single vesicles: mantle isotopic ratios and origin of
637 the air component in basaltic glasses. Earth Planet. Sci. Lett. 274, 142–150.
638 Schwarzenbach, E.M., Gill, B.C., Gazel, E., Madrigal, P., 2016. Sulfur and carbon geochemistry of the Santa Elena peridotites:
639 Comparing oceanic and continental processes during peridotite alteration. Lithos 252–253, 92–108.
640 https://doi.org/http://dx.doi.org/10.1016/j.lithos.2016.02.017
641 Snyder, G., Poreda, R., Fehn, U., Hunt, A., 2003. Sources of nitrogen and methane in Central American geothermal settings:
642 Noble gas and 129I evidence for crustal and magmatic volatile components. Geochemistry, Geophys. Geosystems 4,

1–28.

Staudacher, T., Allègre, C.J., 1988. Recycling of oceanic crust and sediments: the noble gas subduction barrier. Earth Planet. Sci. Lett. 89, 173–183.

Taran, Y.A., 2009. Geochemistry of volcanic and hydrothermal fluids and volatile budget of the Kamchatka–Kuril subduction zone. Geochim. Cosmochim. Acta 73, 1067–1094.

Vaselli, O., Tassi, F., Minissale, A., Montegrossi, G., Duarte, E., Fernandez, E., Bergamaschi, F., 2003. Fumarole migration and fluid geochemistry at Poás volcano (Costa Rica) from 1998 to 2001. Geol. Soc. London, Spec. Publ. 213, 247–262.

Warr, O., Rochelle, C.A., Masters, A., Ballentine, C.J., 2015. Determining noble gas partitioning within a CO2–H2O system at elevated temperatures and pressures. Geochim. Cosmochim. Acta 159, 112–125.

Yeung, L.Y., Li, S., Kohl, I.E., Haslun, J.A., Ostrom, N.E., Hu, H., Fischer, T.P., Schauble, E.A., Young, E.D., 2017. Extreme enrichment in atmospheric 15N15N. Sci. Adv. 3, eaao6741.

Young, E.D., Rumble III, D., Freedman, P., Mills, M., 2016. A large-radius high-mass-resolution multiple-collector isotope ratio mass spectrometer for analysis of rare isotopologues of O2, N2, CH4 and other gases. Int. J. Mass Spectrom. 401, 1–10.

Zelenski, M., Taran, Y., 2011. Geochemistry of volcanic and hydrothermal gases of Mutnovsky volcano, Kamchatka: evidence for mantle, slab and atmosphere contributions to fluids of a typical arc volcano. Bull. Volcanol. 73, 373–394.

Zimmer, M.M., Fischer, T.P., Hilton, D.R., Alvarado, G.E., Sharp, Z.D., Walker, J.A., 2004. Nitrogen systematics and gas fluxes of subduction zones: insights from Costa Rica arc volatiles. Geochemistry, Geophys. Geosystems 5.

Captions

		PO 06-1-3	PO 03-2	Pnar 06-1	PO 06-1-1	PO 06-1-2	ES02 10	Nic-3	Nic-2
		Poas	Poas	Poas	Poas	Poas	Santa Ana	Momotombo	Momotombo
dates of collection		11/5/06	3/31/03	2/24/06	2/24/06	2/24/06		1/5/02	1/5/02
latitude		10.12	10.12	10.12	10.12	10.12	13.5111	12.2519	12.2519
longitude		-84.1359	-84.1359	-84.1359	-84.1359	-84.1359	-89.3748	-86.3224	-86.3224
temperature (Cº)		113	98	153	113	113	400	747	747
quantity of processed N_2	10^{-6} mol	2.1	2.2	8.8	8.0	5.8	22.4		
N_2 vol fraction (ucla)	$x10^{-2}$	9.21E-01	8.47E-01	3.10E-01	7.43E-01	6.01E-01	7.14E-01		
$d^{15}N$	vs. air	-3.69	0.35	-1.38	-1.38	-1.7	0.2	5.41	3.89
D_{30}	vs. stochastic	17	3.43	10.92	10.25	11	15.5	1.5	3.9
1 se $d^{15}N$		0.032	0.018	0.02	0.021	0.022	0.008	0.1	0.1
1 se D_{30}		0.496	0.527	0.288	0.309	0.307	0.138	0.3	0.2
CO_2		0.992	0.990	0.975	0.993	0.990	0.983	0.859	0.861
He		4.56E-05	5.00E-06	5.59E-06	4.97E-06	8.53E-06	6.54E-06	7.61E-06	1.66E-05
H_2		1.17E-04	3.25E-04	1.40E-02	6.62E-05	7.05E-05	4.64E-03	1.24E-01	1.20E-01
Ar		2.42E-04	1.12E-04	1.24E-04	3.10E-04	4.21E-04	9.98E-05	1.52E-04	3.70E-05
O_2		4.19E-04	1.25E-05	1.45E-04	5.28E-04	7.90E-04	4.54E-06	1.14E-05	8.93E-06
N_2		6.70E-03	1.00E-02	1.06E-02	6.56E-03	8.94E-03	1.20E-02	1.62E-02	1.88E-02
CH_4		6.44E-06	1.25E-06	1.20E-04	7.24E-06	9.48E-06	1.95E-05	8.88E-06	7.66E-06
He/Ar		1.89E-01	4.44E-02	4.50E-02	1.60E-02	2.03E-02	6.55E-02	5.00E-02	4.48E-01
N_2/He		1.47E+02	2.00E+03	1.91E+03	1.32E+03	1.05E+03	1.83E+03	2.13E+03	1.13E+03
N_2/Ar		2.77E+01	8.89E+01	8.58E+01	2.11E+01	2.12E+01	1.20E+02	1.07E+02	5.07E+02
O_2/N_2		6.25E-02	1.25E-03	1.36E-02	8.04E-02	8.83E-02	3.80E-04	7.03E-04	4.76E-04
N_2/CH_4		1.04E+03	8.00E+03	8.87E+01	9.06E+02	9.43E+02	6.14E+02	1.83E+03	2.45E+03
$^{40}Ar/^{36}Ar$					297	293		305	
$^3He/^4He$	(R_A)	6.44	7.15	6.96	7.15	7.15	7.56	6.99	6.99
$N_2/^3He$		1.63E+07	2.00E+08	1.96E+08	1.32E+08	1.05E+08	1.73E+08	2.18E+08	1.16E+08
$N_2/^{36}Ar$		8.49E+03	2.72E+04	2.62E+04	6.47E+03	6.49E+03		3.26E+04	1.78E+05
$^4He/^{20}Ne$		8.93E+00	1.90E+02	3.61E+02	1.56E+02	1.56E+02	6.66E+01	2.75E+02	2.75E+02
$^3He/^{22}Ne$		8.04E-04	1.90E-02	3.52E-02	1.56E-02	1.56E-02	7.05E-03	2.69E-02	2.69E-02
X value		28	596	1133	488	488	209	864	864
$^3He/^{36}Ar$		5.20E-04	1.36E-04	1.34E-04	4.90E-05	6.20E-05		1.50E-04	
$^4He/^{40}Ar$		1.89E-01	4.46E-02	4.51E-02	1.61E-02	2.03E-02		5.02E-02	

Table 1. Nitrogen and light noble gases isotope and concentrations for central Americans fumaroles

sample ID		LH180406	CL180409	CH180410	PX180416	PS180405	BS180407	HA180403	CW180415	XF180416
spring name		Los Pozos	Colobre	Chiguiri Abajo	San Juan PraxAir	Playa Sandalo	Bajo Mended	Hatillo	Cauhita	San Juan PraxAir
latitude		8.870954	8.404478	8.705078	10.488755	8.575544	8.66645	9.360224	9.735746	10.485523
longitude		-82.689901	-80.803745	-80.269193	-84.113598	-83.36416	-82.349098	-83.916639	-82.825737	-84.113229
temperature (C⁹)		55	51	31	29	31	41	33	35	29
quantity of processed N_2	10^{-6} mol	18.0	540.0	7.2	38.0	28.0	588.0	556.0	39.2	2.8
N_2 vol fraction (ucla)	$x10^{-2}$	2.89E-02	8.67E-01	1.16E-02	6.10E-02	4.49E-02	9.44E-01	8.92E-01	6.29E-02	4.49E-03
$d^{15}N$	vs. air	-1.38	0.55	1.60	0.20	0.71	4.19	0.22	0.34	1.30
D_{30}	vs. stochastic	18.39	15.27	12.52	19.35	18.42	8.73	7.29	18.47	15.09
1 se $d^{15}N$		0.029	0.004	0.028	0.007	0.008	0.004	0.004	0.004	0.031
1 se D_{30}		0.825	0.099	0.563	0.22	0.24	0.168	0.077	0.097	0.617
CO_2		0.997	0.018	0.985	0.944	0.082		0.031	0.054	
He		1.47E-07	4.98E-04	1.54E-05	1.97E-06	1.90E-06		4.19E-04	1.04E-05	
H_2		9.07E-07	3.92E-06	1.77E-07	9.81E-08	1.51E-05		7.48E-05	1.62E-05	
Ar		4.79E-05	1.12E-02	3.76E-04	3.52E-04	1.07E-03		6.90E-03	1.71E-03	
O_2		5.75E-04	4.78E-03	1.87E-03	1.19E-02	2.77E-03		3.12E-02	1.10E-02	
N_2		2.04E-03	9.63E-01	1.32E-02	4.41E-02	5.03E-02		9.30E-01	9.92E-02	
CH_4		9.62E-08	2.52E-03	4.53E-05	2.66E-06	8.64E-01		3.09E-04	8.34E-01	
He/Ar		3.07E-03	4.46E-02	4.09E-02	5.60E-03	1.77E-03	2.57E-03	6.07E-02	6.09E-03	3.85E-02
N_2/He		1.39E+04	1.93E+03	8.54E+02	2.23E+04	2.65E+04	4.23E+04	2.22E+03	9.56E+03	1.21E+03
N_2/Ar		4.27E+01	8.62E+01	3.50E+01	1.25E+02	4.69E+01	1.09E+02	1.35E+02	4.64E+01	4.64E+01
O_2/N_2		2.81E-01	4.96E-03	1.42E-01	2.69E-01	5.50E-02		3.36E-02	1.11E-01	
N_2/CH_4		2.12E+04	3.83E+02	2.91E+02	1.65E+04	5.82E-02		3.01E+03	1.19E-01	
^{4}He	$x10^{-9}$ cc/ccSTP	3.21E+01	4.39E+05	1.28E+04	1.12E+03	1.65E+02	2.23E+04	3.98E+05	4.40E+03	3.72E+03
^{20}Ne	$x10^{-9}$ cc/ccSTP	2.24E+00	1.37E+04	1.23E+02	6.81E+02	3.98E+02	1.58E+04	7.07E+03	6.15E+02	5.85E+01
^{40}Ar	$x10^{-6}$ cc/ccSTP	3.85E+00	1.15E+04	3.59E+02	3.95E+02	4.83E+02	8.67E+03	6.35E+03	7.49E+02	9.65E+01
^{36}Ar	$x10^{-9}$ cc/ccSTP	1.28E+01	3.74E+04	1.05E+03	1.29E+03	1.59E+03	2.67E+04	2.06E+04	2.43E+03	3.16E+02
^{40}Ar/^{36}Ar		301	308	342	305	304	325	308	309	306
^{3}He/^{4}He	(R_A)	7.48	8.78	6.37	6.52	1.55	0.27	1.82	2.05	7.59
^{20}Ne/^{22}Ne		10.00	9.83	9.89	9.82	9.84		9.85	9.87	9.91
^{21}Ne/^{22}Ne		0.023	0.029	0.029	0.029	0.029		0.029	0.029	0.029
N_2/^{3}He		1.33E+09	1.57E+08	9.59E+07	2.45E+09	1.22E+10	1.12E+11	8.72E+08	3.33E+09	1.14E+08
N_2/^{36}Ar		1.29E+04	2.66E+04	1.20E+04	3.83E+04	1.43E+04	3.53E+04	4.17E+04	1.80E+04	1.42E+04
^{4}He/^{20}Ne		1.43E+01	3.21E+01	1.04E+02	1.65E+00	4.15E-01	1.41E+00	5.63E+01	7.15E+00	6.37E+01
^{3}He/^{22}Ne		1.50E-03	3.87E-03	9.19E-03	1.48E-04	8.85E-06	5.34E-06	1.41E-03	2.02E-04	6.70E-03
X value		45	101	327	5	1	4	177	22	200
^{3}He/^{36}Ar		9.70E-06	1.69E-04	1.25E-04	1.57E-05	1.17E-06	3.16E-07	4.78E-05	5.41E-06	1.25E-04
^{4}He/^{40}Ar		3.08E-03	4.47E-02	4.10E-02	5.62E-03	1.77E-03	2.50E-03	6.09E-02	6.11E-03	

Table 2 Nitrogen and light noble gases isotope and concentrations for central American springs

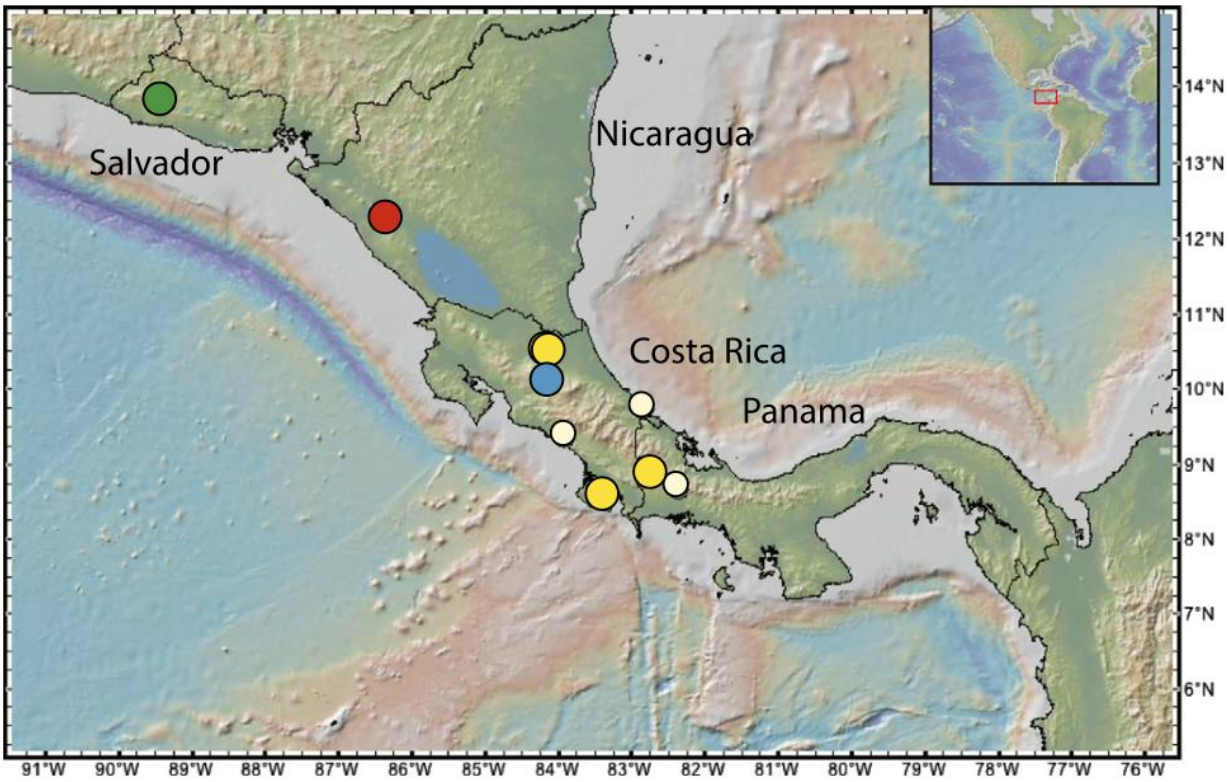

672

673 **Fig. 1: location of all the samples studied here.**
674 Green, red and blue symbols are fumarole locations from Santa Ana, Momotombo and Poás
675 (Data in table 1). Yellow symbols are springs (Data in table 2).

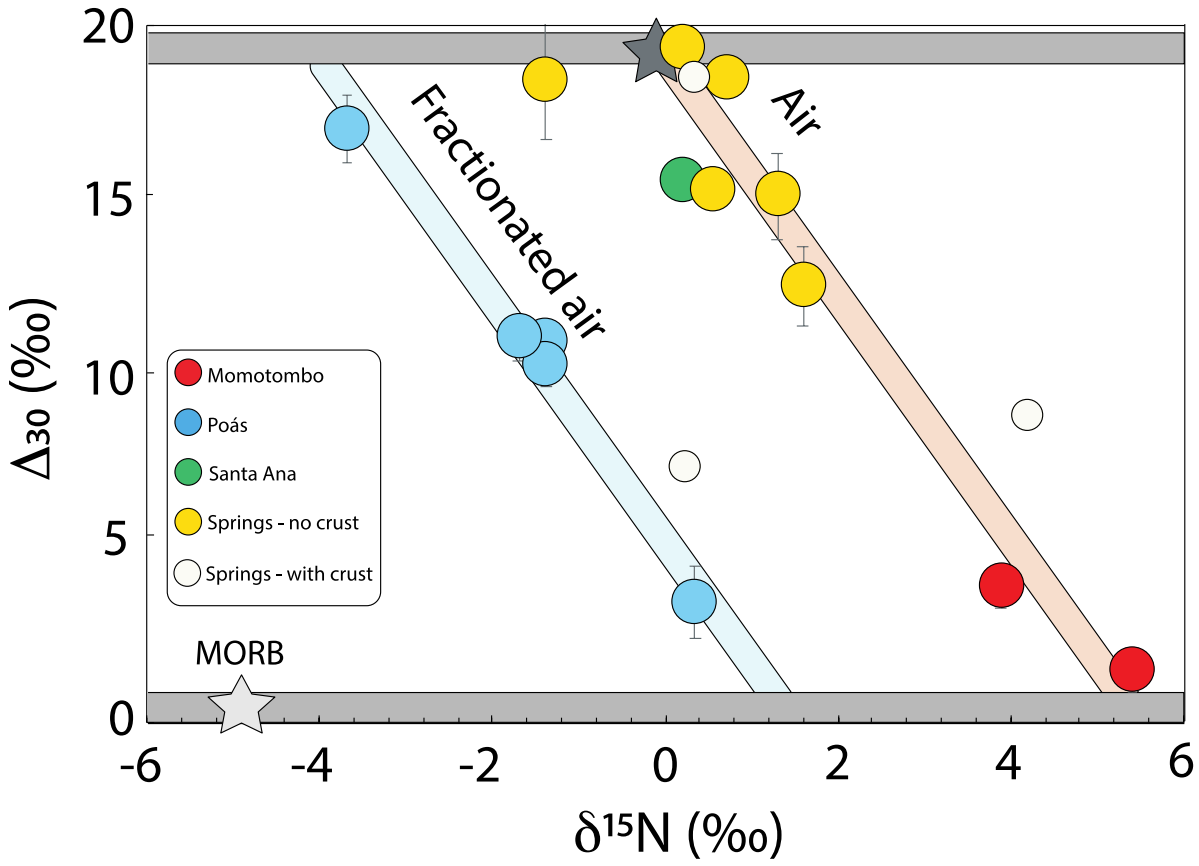

Fig. 2 the nitrogen isotopic composition of volcanic discharges in central America. Variable Δ_{30} values establish that our samples incorporate variable amounts of atmospheric nitrogen. Fumaroles from the Poás and Momotombo have the lowest Δ_{30} values indicating they have the lowest air-derived N_2 contributions while the hot springs from Costa Rica have the highest air contributions. Variable $\delta^{15}N$ values are observed, between -3.7±0.3‰ and +4.2±0.3‰. At an air Δ_{30} values, variable $\delta^{15}N$ must be caused by a mass-dependent isotope fractionation, presumably associated with hydrothermal degassing. The high-temperature components have positive $\delta^{15}N$ values.

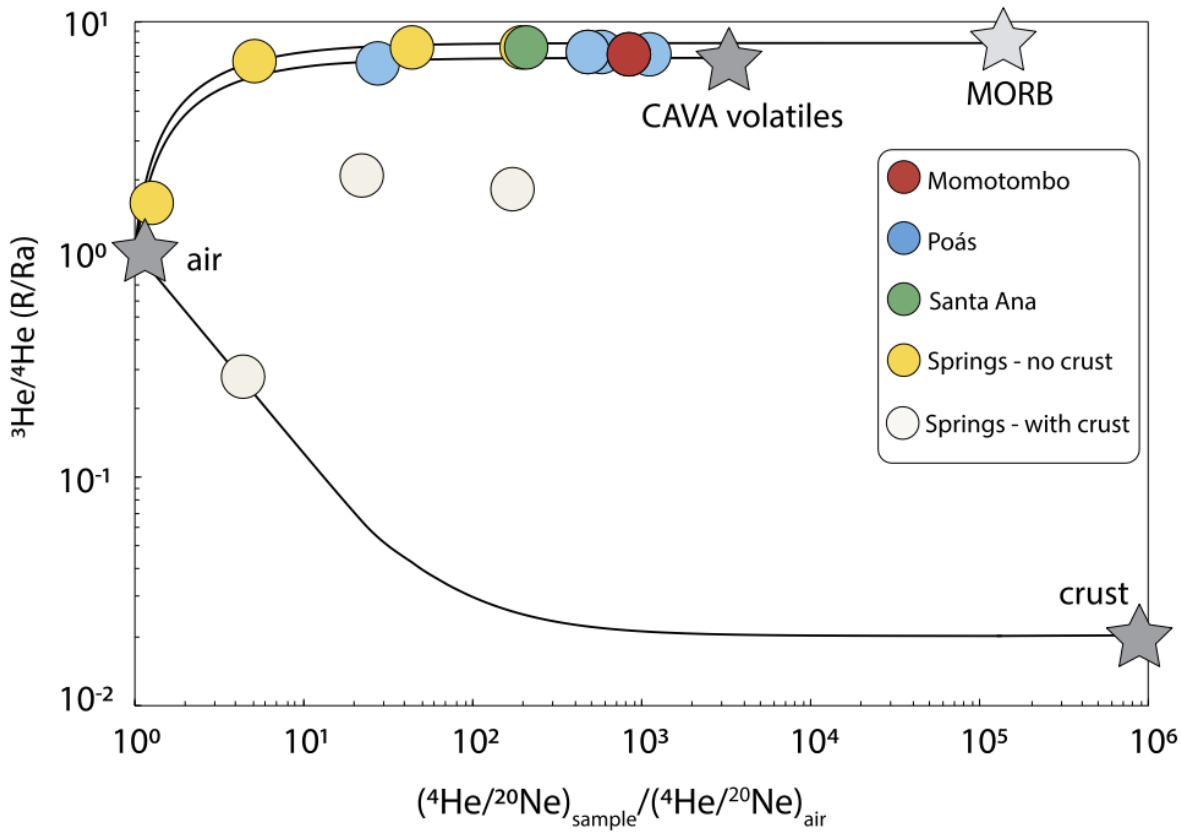

686

687 **Fig. 3: Measured $^{3}He/^{4}He$ ratios versus $^{4}He/^{20}Ne$ ratios of the samples, normalized to air by**
688 **convention (De Leeuw et al, 2007).** Most samples indicate simple two-component air-magma
689 mixing. Three Costa Rica hot springs (HS) however show additions of crustal ^{4}He.

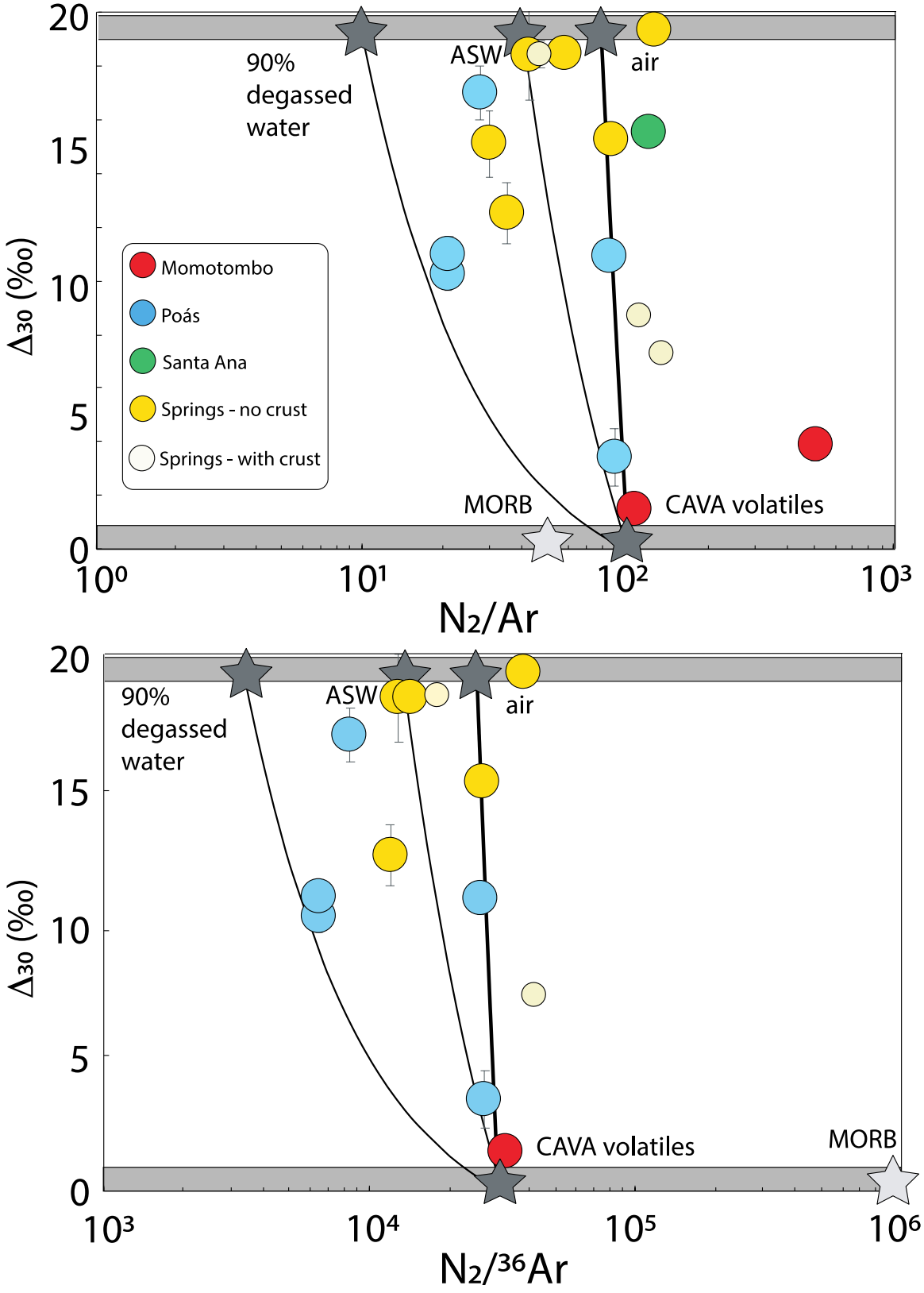
20
15
10
5
0
Δ30 (‰)
90%
degassed
water
ASW
air
Momotombo
Poás
Santa Ana
Springs - no crust
Springs - with crust
MORB
CAVA volatiles
10⁰
10¹
10²
10³
N2/Ar
20
15
10
5
0
Δ30 (‰)
90%
degassed
water
ASW
air
CAVA volatiles
MORB
10³
10⁴
10⁵
10⁶
N2/36Ar

690

Fig. 4: Measured N_2/Ar and $N_2/^{36}$Ar ratios versus Δ_{30} values. Mixing lines are shown for mixtures between the high-temperature component observed at both Momotombo and Poás, and variably fractionated atmospheric components, including air, air-saturated water (ASW), and degassed water. The high-temperature endmembers with Δ_{30} = 0‰ defined by the data from Momotombo and Poás have similar N_2/Ar and $N_2/^{36}$Ar ratios of ~ 100 and ~ 10^4, respectively. Here, we adopt values of ~100 and 3 x 10^4 for N_2/Ar and $N_2/^{36}$Ar ratios for the high-T endmember at Momotombo. Nitrogen and argon have indistinguishable solubilities in silicate melts and thus are not fractionated by magmatic degassing at ~1200 °C (Libourel et al., 2003). Thus, the low $N_2/^{36}$Ar at Momotombo is not resulting from fractionations during magmatic degassing. Instead, it may be a feature of the Momotombo mantle source. At Poás, fumarole samples are consistent with the same N_2/Ar ratio for the high-temperature component as at Momotombo. If hydrothermal degassing affected the high-T volatiles at Poás, the pristine N_2/Ar and $N_2/^{36}$Ar for high-T gases at Poás could be higher than the observed values. Note that combining a ^{3}He/^{36}Ar ratio of ~ 10^{-4} (see Fig. 6B) to the observed $N_2/^3$He of ~ 10^8 (Fig. 4) returns to a $N_2/^{36}$Ar of ~ 10^4, consistent with the conclusion of a low N_2/Ar in our sampling of high-temperature endmembers (see section 5.4).

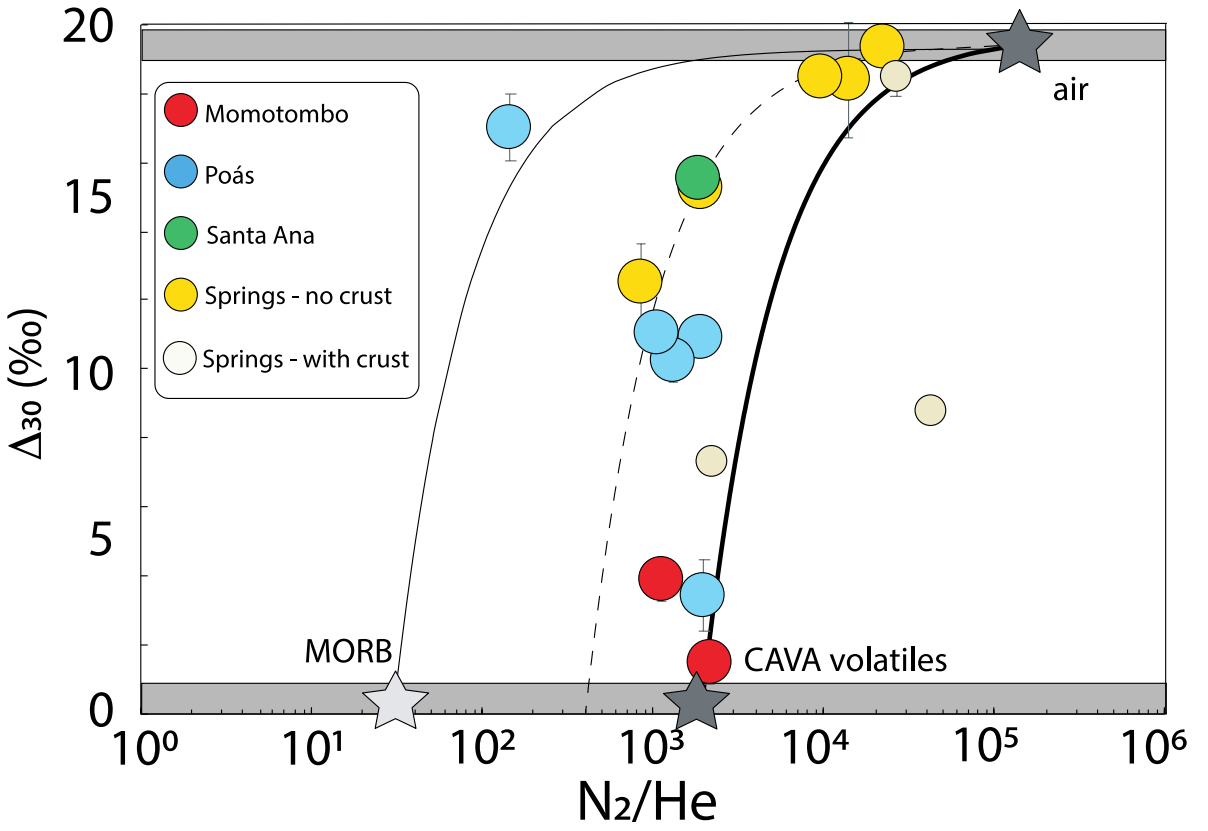
Momotombo
Poás
Santa Ana
Springs - no crust
Springs - with crust
air
MORB
CAVA volatiles
Δ30 (‰)
N2/He

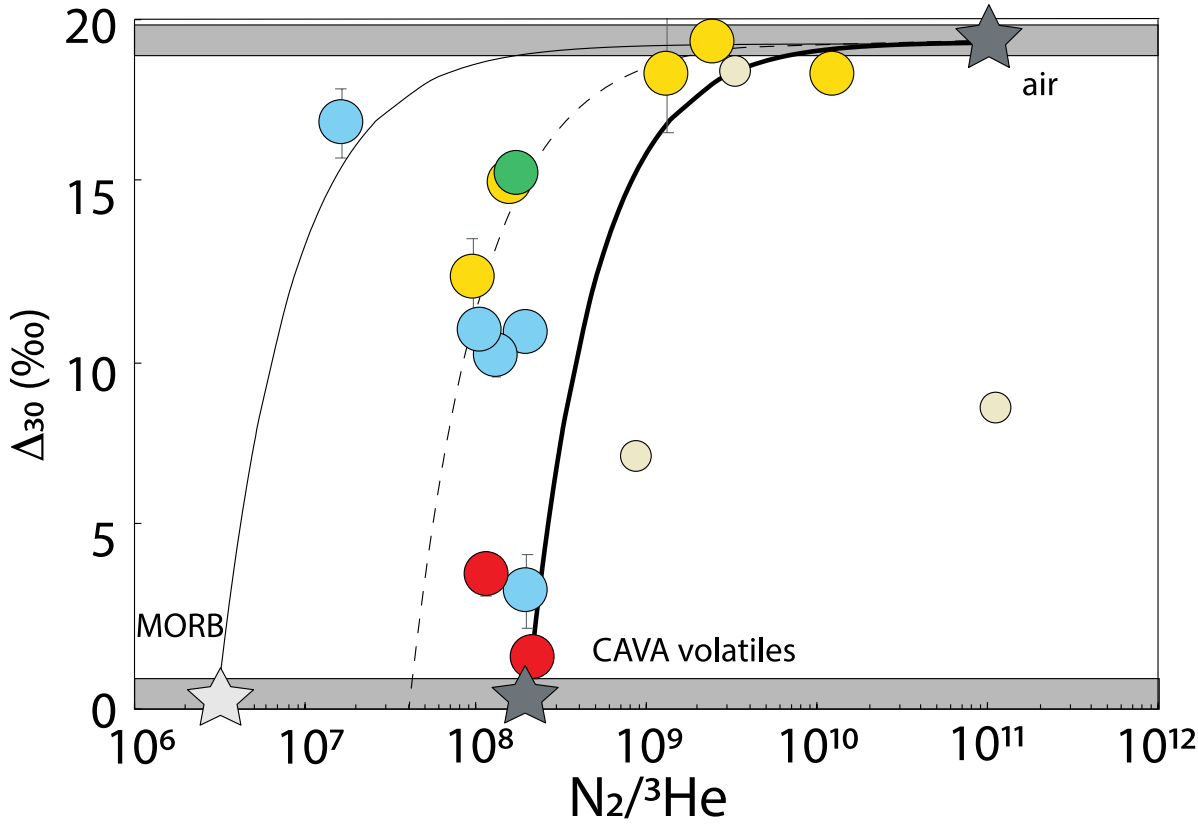
air
MORB
CAVA volatiles
Δ30 (‰)
N2/3He

709

Fig. 5: Measured N_2/He and $N_2/^3$He ratios versus Δ_{30} values. Mixing lines are shown for mixtures between air and three high-temperature components: MORBs, and two variably N_2-enriched endmembers required to fit the data. Springs with additions of crustal ^{4}He are shown in the smallest symbols. They are not used for fluxes calculations – see discussion in the supplementary discussion.

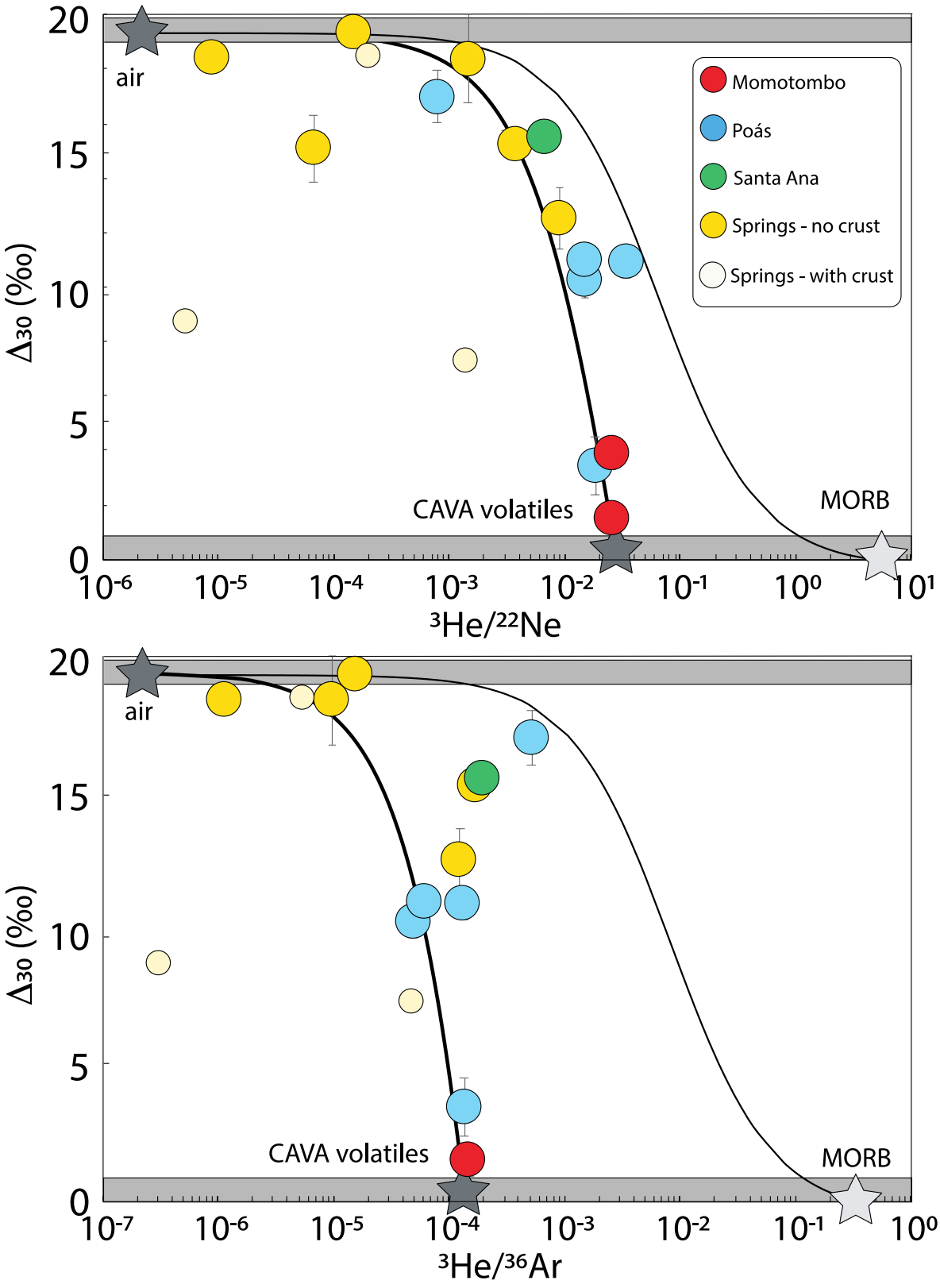
air
CAVA volatiles
MORB
Momotombo
Poás
Santa Ana
Springs - no crust
Springs - with crust
Δ30 (‰)
3He/22Ne
3He/36Ar

715

Fig. 6: Measured $^{3}He/^{22}Ne$ and $^{3}He/^{36}Ar$ ratios versus Δ_{30} values. Springs with additions of crustal ^{4}He are shown in the smallest symbols. They are not used for fluxes calculations – see discussion in the supplementary discussion. Mixing lines are the same as in figure 3 and 4. They are shown for mixtures between air and high-temperature components: MORB, and a N_2-^{36}Ar-^{22}Ne enriched endmember that fits the data. The mixing relationships are curved because of the logarithm scale, but also because of how distinct the N_2/Ne of the mixing endmembers may be. Air has a $N_2/^{20}Ne$ ratio of air is 4.5×10^4. For MORB, we calculate a the $N_2/^{20}Ne$ of 1.3×10^6. This is based on a $N_2/^{3}He$ of 3×10^6 for the MORB mantle (Javoy and Pineau, 1991). We combine this $N_2/^{3}He$ estimate with $^{3}He/^{4}He$ and $^{4}He/^{20}Ne$ values for the MORB mantle from Moreira et al (1998). Using the $^{3}He/^{22}Ne$ ratio of the MORB mantle (Moreira et al., 1998), we derive a $N_2/^{22}Ne$ of 1.7×10^7. Conversely, we here derive $N_2/^{3}He$, $^{3}He/^{22}Ne$ ratios of the central American high-temperature volatiles. Combining those with $^{3}He/^{4}He$ of ~7 from Fig. 3, we derive $N_2/^{20}Ne$ and $N_2/^{22}Ne$ ratios of 3.4×10^5 and 3.3×10^6, respectively. On panel b, the curvatures are function the N_2/Ar of the mixing endmembers, which are estimated on Fig. 4.

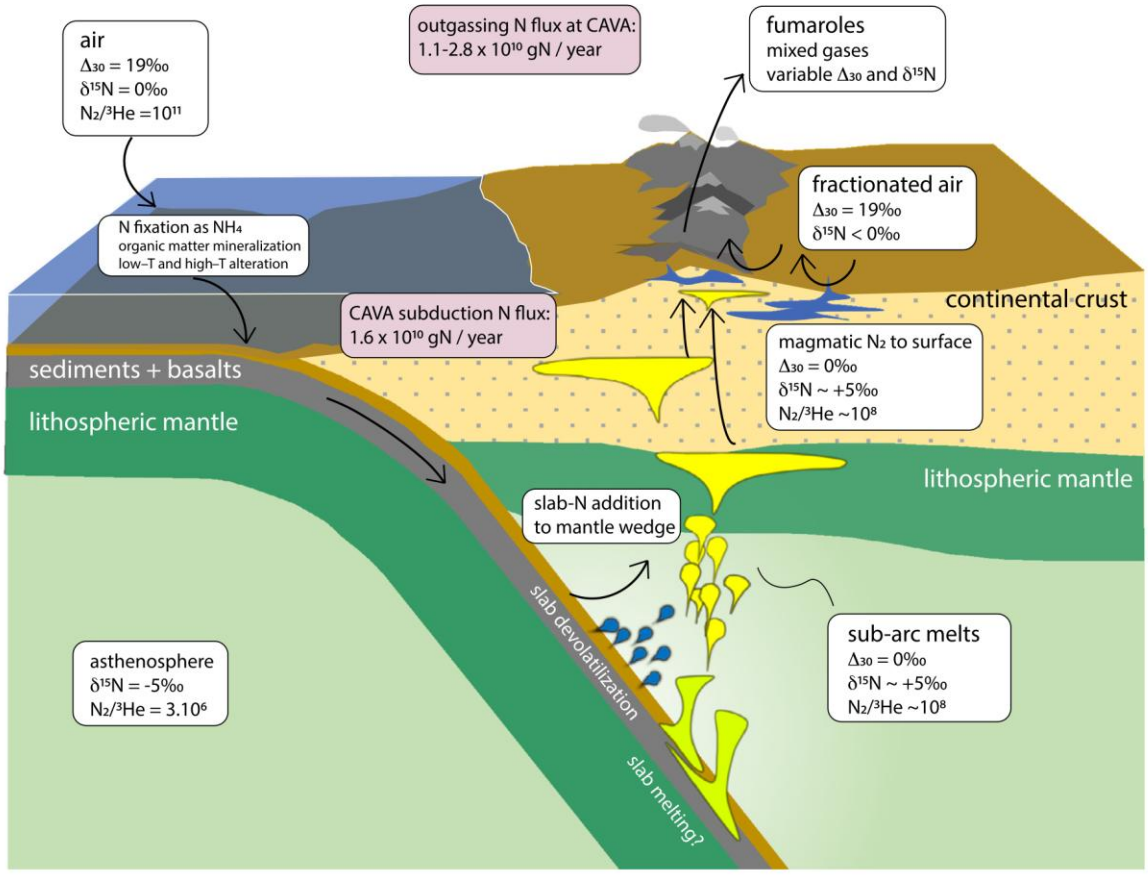

Fig. 7 Cartoon representing various processes and reservoirs constrained in this study. Scales are grossly exaggerated, especially for melt conduits and magma chambers. A slab with sediments, basalts, and oceanic lithospheric mantle is shown to enter subduction. The slab composition is not constrained here but is likely enriched in all volatiles relative to ^{3}He (Busigny et al., 2019, Chavrit et al., 2016). In the slab, nitrogen is fixed as NH_4^+ (Busigny et al., 2019 and

737 references therein) so no Δ_{30} values are defined; Δ_{30} is only relevant for N_2 molecules. Both slab
738 devolatilization and slab melting are shown for illustration. Any slab melting would be relevant
739 underneath Costa Rica (Hoernle et al., 2008) while slab devolatilization and sediment-derived
740 fluids would contribute to sources underneath Nicaragua and El Salvador (Patino et al., 2000).
741 The melting region is characterized as the high-temperature endmembers constrained in this
742 work (Fig. 7). Melts and super-critical fluids are suggested to host dissolved N_2 (Libourel et al.,
743 2003; Mikhail and Sverjensky, 2014). Upon partial melting of a NH_3-bearing mantle source,
744 magmatic N_2 would form with a Δ_{30} of 0‰. The high-T N_2 is then contributed to hydrothermal
745 systems in the sub-surface by near-quantitative magmatic degassing. Air circulation in the sub-
746 surface allows air-saturated waters to undergo degassing, and subsequent gas release with
747 fractionated compositions.
748

749